

Simulating global properties of electroencephalograms with minimal random neural networks

Peter beim Graben^{a,b,*}, Jürgen Kurths^b

^a*School of Psychology and Clinical Language Sciences, University of Reading, UK*

^b*Institute of Physics, Nonlinear Dynamics Group, Universität Potsdam, Germany*

Received 30 March 2006; received in revised form 7 December 2006; accepted 9 February 2007

Communicated by V. Jirsa

Available online 16 March 2007

Abstract

The human electroencephalogram (EEG) is globally characterized by a $1/f$ power spectrum superimposed with certain peaks, whereby the “alpha peak” in a frequency range of 8–14 Hz is the most prominent one for relaxed states of wakefulness. We present simulations of a minimal dynamical network model of leaky integrator neurons attached to the nodes of an evolving directed and weighted random graph (an Erdős–Rényi graph). We derive a model of the dendritic field potential (DFP) for the neurons leading to a simulated EEG that describes the global activity of the network. Depending on the network size, we find an oscillatory transition of the simulated EEG when the network reaches a critical connectivity. This transition, indicated by a suitably defined order parameter, is reflected by a sudden change of the network’s topology when super-cycles are formed from merging isolated loops. After the oscillatory transition, the power spectra of simulated EEG time series exhibit a $1/f$ continuum superimposed with certain peaks.

© 2007 Elsevier B.V. All rights reserved.

Keywords: EEG; Field potentials; Leaky integrator units; Random graphs; Phase transitions; Order parameter

1. Introduction

The electrical activity of the brain can be measured with the electroencephalogram (EEG). Its origin is due to the synchronized activity of large formations of cortical neurons, the pyramidal cells. These nerve cells possess an axial symmetry and they are aligned in parallel perpendicular to the surface of the cortex thus forming a palisade of cell bodies and dendritic trees [11,45]. They receive excitatory input at the superficial apical dendrites from thalamic relay neurons and inhibitory input at the basal dendrites and at their somata from local interneurons [11,45,18]. Excitatory and inhibitory synapses cause different ion currents through their cell membranes thus leading to either depolarization or hyperpolarization,

respectively. When these synapses are activated, a single pyramidal cell behaves as a microscopic electric dipole surrounded by its characteristic dendritic field in the extracellular space. The *dendritic field potentials* (DFP) of a large assembly of cortical pyramidal cells superimpose to the *local field potential* (LFP) of a dipole layer which eventually contributes to the EEG measurable at the human’s scalp [11,56,5,40].

One of the most obvious features of the EEG are oscillations in certain frequency bands. The *alpha waves* are sinusoidal-like oscillations between 8 and 14 Hz, strongly pronounced over parietal and occipital recording sites which reflect a state of relaxation during wakefulness, with no or only low visual attention. Alpha waves are related to awareness and cognitive processes [41,4,30,47]. In the power spectrum of the EEG, these oscillations are represented by particular peaks superimposed to a broad-band $1/f$ continuum [11,7].

The $1/f$ behavior and the existence of distinguished oscillations in the EEG such as the alpha waves are cornerstones to evaluate computational models of the

*Corresponding author. School of Psychology and Clinical Language Sciences, University of Reading, Whiteknights, P.O. Box 217, Reading RG6 6AH, UK. Tel.: +440118 378 6105.

E-mail addresses: p.r.beimgraben@reading.ac.uk (P. beim Graben), jkurths@gmx.de (J. Kurths).

EEG. Yet, modeling these brain rhythms has a long tradition. Wilson and Cowan [53] were the first who used a population model of excitatory and inhibitory neurons that innervate each other. They introduced a two-dimensional state vector whose components describe the proportion of firing McCulloch–Pitts neurons [38] within a unit volume of neural tissue at an instance of time. Lopez da Silva et al. [35] pursued two different approaches: a distributed model of the thalamus where relay cells and interneurons are considered individually, and a “lumped” model analogous to the neural mass model of Wilson and Cowan [53]. Lopez da Silva et al. [35,36] were able to show that their model reproduces a peak around 10 Hz, i.e. “alpha waves”, in the spectrum.

The neural mass model [35] has been further developed by Freeman [17], Jansen et al. [24,25], Wendling et al. [51,52], and researchers from the Friston group [12–14] in order to model the EEG of the olfactory system, epileptic EEGs, and event-related potentials (ERP), respectively.

On the other hand, Rotterdam et al. [50] generalized the model [35] to spatiotemporal dynamics by considering a chain of coupled cortical oscillators. A similar approach has been pursued by Wright and Liley [55,54] who discussed a spatial lattice of coupled unit volumes of excitatory and inhibitory elements obeying cortical connectivity statistics. The most important result that we shall appreciate here is that the power spectrum exhibits the alpha peak, and that there is a shift of that peak towards the beta band with increasing input describing arousal.

Moreover, Liley et al. [34] suggested a distributed model of cortical alpha activity using a compartmental description of membrane potentials [31]. In such an approach, nerve cells are thought to be built up by cylindrical compartments that are governed by generalized Hodgkin–Huxley equations [21]. Liley et al. [34] reported two oscillatory regimes of this dynamics: one having a broad-band spectrum with a peak in the beta range of about 20 Hz, and the other narrowly banded with a peak around the alpha frequency.

Surveying these attempts, one recognizes two main lines of research. In the first approach, relatively small networks of neurons, or even of neural masses, are hand-crafted in order to meet anatomical and physiological constraints [1,16,17,34–36,50–55,24,25,12–14]. In the second one, statistical properties of the nervous tissue are treated by field theoretical approaches [40,28,26,42,43,56,57]. Yet, the recent developments of random graph theory describing networks with complex topology [2,10,9,39,23,8,44,46,29] suggest a third, medial, way of brain modeling using complex networks whose nodes are attached to dynamical neuron models [46,27,48,22,58,32].

In this paper, we shall pursue this third approach by proposing a *minimal dynamical network model* where the onset of oscillatory behavior is correlated with the emergence of super-cycles in the network’s topology. The network is provided by an evolving directed and weighted Erdős–Rényi graph of N nodes where all connections

between two nodes are equally likely with increasing probability [2,10,9]. To each node of the graph a simple neuron model, the *leaky integrator neuron*, is attached [53,20,33,22].

2. Minimal random neural networks

In this section, we describe our minimal neural network model, namely an evolving directed and weighted Erdős–Rényi graph. The nodes of this most simple network type are occupied by a rather simple neuron model, the leaky integrator unit. We argue that the net input to such a unit can be regarded as a rough approximation of the DFP, and demonstrate how the superposition of the DFPs of a neural mass give rise to an estimator of the LPF. Finally, the superposition of the LFPs should be considered as our model EEG.

2.1. A minimal network model

A directed Erdős–Rényi graph consists of a set of vertices V that are randomly connected by arrows taken from an edge set $E \subset V \times V$ with equal probability q . The topology of the graph is completely described by its *adjacency matrix* $\mathbf{A} = (a_{ij})$ where $a_{ij} = 1$, if there is an arrow connecting the vertex j with the vertex i (i.e. $(j, i) \in E$ for $i, j \in V$) while $a_{ij} = 0$ otherwise. A directed and weighted Erdős–Rényi graph is then described by the *weight matrix* $\mathbf{W} = (w_{ij})$ which is obtained by element-wise multiplication of the adjacency matrix with constants g_{ij} , $w_{ij} = g_{ij}a_{ij}$.

The weights w_{ij} may be positive or negative. In the former case the connection $j \rightarrow i$ is called *excitatory*, in the latter *inhibitory*. Biologically plausible models must satisfy Dale’s law saying that excitatory neurons have only excitatory synapses while inhibitory neurons only possess inhibitory synapses [15]. Therefore, the column vectors of the weight matrix are constrained to unique sign. We meet this requirement by randomly choosing a proportion p of the vertices to be excitatory and the remainder to be inhibitory.

In our model the weights become time-dependent due to the following evolution algorithm:

- (i) Initialization: $\mathbf{W}(0) = 0$.
- (ii) At evolution time t , select a random pair of nodes i, j .
- (iii) If they are not connected, create a synapse with weight $w_{ij}(t+1) = \delta_{\text{ex}}$ if j is excitatory, and $w_{ij}(t+1) = \delta_{\text{in}}$ if j is inhibitory. If they are already connected, enhance the weight $w_{ij}(t+1) = w_{ij}(t) + \delta_{\text{ex}}$ if $w_{ij}(t) > 0$ and $w_{ij}(t+1) = w_{ij}(t) + \delta_{\text{in}}$ if $w_{ij}(t) < 0$. All other weights remain unchanged.
- (iv) Repeat from (ii) for a fixed number of iterations L .

For the excitation-to-inhibition ratio for balanced activity [49] to be of the order of magnitude of 1:4 [42], we chose as the “learning rates” $\delta_{\text{ex}} = +1$ for excitatory synapses and

$\delta_{in} = -4$ for inhibitory synapses. Note that this algorithm is not intended to describe synaptic plasticity, but rather to give a minimal description of brain development where the connectivity evolves during the time L .

2.2. A minimal neuron model

Our minimal dynamical neural network model comprises the simple topology described in Section 2.1 and moreover a simple dynamics that will be derived in the sequel.

We consider the somatic membrane potentials $V_i(t)$ of the i th neuron in the vicinity of its axon hillock as the state variables of the model. The gradient between the post-synaptic potential \tilde{V}_{ij} at the synapse connecting neuron j with neuron i and the potential V_i at the trigger zone of neuron i drives the current

$$I_{ij} = \frac{\tilde{V}_{ij} - V_i}{r_{ij}} \quad (1)$$

through the somato-dendritic cell plasma with resistance r_{ij} . The superposition of these currents flows from the axon hillock into the extracellular space thereby dropping to the membrane potential $V_i(t)$ that obeys Kirchhoff's law

$$\sum_j I_{ij} = \frac{V_i - V_m}{r_m} + c_i \frac{dV_i}{dt}, \quad (2)$$

where V_m denotes the Nernst equilibrium potential (which we deliberately equal to zero subsequently) of the cell membrane with resistance r_m and c_i is the membrane's capacitance.

Inserting Eq. (1) into Eq. (2) substitutes I_{ij} with the postsynaptic potentials \tilde{V}_{ij} . These are obtained by the convolution products

$$\tilde{V}_{ij}(t) = S_{ij}(t) * R_j(t) \quad (3)$$

of the spike train $R_j(t)$ arriving at the presynaptic terminal of neuron j with a postsynaptic impulse response function $S_{ij}(t)$, which is usually described as an alpha function [31,15]. Yet, for the sake of simplicity, we shall approximate

$$S_{ij}(t) = g_{ij} \delta(t), \quad (4)$$

where g_{ij} is the gain factor of the synapse between neuron j and i , and $\delta(t)$ denotes Diracs's distribution.

Finally, we have to express the spike rate $R_j(t)$ by the state variable V_j of the presynaptic neuron j that is given by the logistic function

$$R_j(t) = f(V_j(t)) = \frac{1}{1 + \exp[-\beta_j(V_j(t) - \theta_j)]} \quad (5)$$

with the parameters gain β_j and threshold θ_j [3].

From Eqs. (1)–(5) we obtain the basic equation of the leaky integrator neuron [53,20,33,22],

$$\tau_i \frac{dV_i}{dt} + V_i = \sum_j w_{ij} f(V_j(t)) \quad (6)$$

with time constants

$$\tau_i = \frac{r_m c_i}{1 + \sum_j (r_m / r_{ij})}$$

and synaptic weights

$$w_{ij} = g_{ij} \frac{r_m / r_{ij}}{1 + \sum_j (r_m / r_{ij})}.$$

The DFP of the i th neuron is proportional to the total synaptic current flowing through its membrane into the extracellular space and returning back to the soma [56,5]. In our model, the DFP is estimated by net input

$$D_i(t) = \sum_j w_{ij} f(V_j(t)) \quad (7)$$

to neuron i . It describes the amount of excitation ($w_{ij} > 0$) minus the contribution of inhibition ($w_{ij} < 0$) [24,25,51,52,12–14,56,5].

2.3. A minimal neural mass model

The dynamics of a minimal random neural network resulting from the evolution algorithm described in Section 2.1 is governed by the differential equation (6). Following Freeman [16,17], neural networks can be regarded as being hierarchically composed from neural masses. For two such populations of either mutually connected excitatory or inhibitory neurons (Freeman's "KI_e" and "KI_i sets") the sum in the r.h.s. of Eq. (6) could be split into the difference of two sums

$$\sum_j w_{ij} f(V_j(t)) = \sum_{j^+} w_{ij}^+ f(V_{j^+}(t)) - \sum_{j^-} |w_{ij}^-| f(V_{j^-}(t)), \quad (8)$$

where w_{ij}^+ are the positive and w_{ij}^- are the negative weights and the indices j^+, j^- indicate whether the neuron j belongs to the excitatory KI_e set or to the inhibitory KI_i set. This decomposition corresponds to the formation of a KII set in Freeman's notation. Note that a neuron with index j^+ from the KI_e set can project into both populations $i \in$ KI_e and $i \in$ KI_i, and correspondingly for j^- . Therefore, the mass is a full KII set and not only its reduced counterpart [16].

Since also the global gain function f for both populations is given by the logistic function (Eq. (5)) [53,18], the difference equation (8) obeys

$$f(x) - f(y) = \frac{1}{2} \left[\tanh\left(\frac{x}{2}\right) - \tanh\left(\frac{y}{2}\right) \right]. \quad (9)$$

Therefore, Eq. (6) describes both single neurons with logistic activation functions (Eq. (5)) and also whole KII populations with hyperbolic tangent gain functions. Hence in the present study, we chose $f_i(x) = \tanh x$ for all $1 \leq i \leq N$ thereby modeling a random network of neural masses.

In our approach, the DFP was estimated by Eq. (7). Likewise, the LFP of a neural population i is approximated

by the same expression

$$F_i(t) = \sum_j w_{ij} f_i(V_j), \quad (10)$$

where V_j describes now the mass activity and f is given by the hyperbolic tangent rather than the logistic function.

In order to compute the model EEG, we finally take the sum of the LFPs of all KII populations that excite other masses

$$E(t) = \sum_{i^+} F_i(t). \quad (11)$$

It is easy to recognize that Eq. (6) can be used to implement a neural oscillator by taking two nodes, one excitatory and the other inhibitory. Choosing an antisymmetric weight matrix $w_{12} = -w_{21}$ and a linear gain function $f(x) = x$, Eq. (6) simply describes a damped harmonic oscillator. This raises the question whether oscillators emerge in random neural networks that evolve according to the algorithm presented in Section 2.1.

3. Simulations

This question is addressed by our simulations. To begin with, we create networks of increasing size of $N = 200, 500$, and 1000 nodes. Since about 80% of cortical neurons are excitatory pyramidal cells, we assume that also $p = 80\%$ of the network's nodes (i.e. the neural masses) are excitatory. For each iteration of the network's evolution, the dynamics of its nodes is examined. After preparing them with normally distributed initial conditions ($\mu = 0, \sigma = 1$), Eq. (6) is solved numerically for an ensemble of $K = 10$ time series of length $T = 100$ comprising 4069 samples. LFP and EEG are computed according to Eqs. (10) and (11). In order to further simplify the simulations, we set $\tau_i = 1, \beta_i = 1, \theta_i = 0$ for all $1 \leq i \leq N$.

From the simulated EEGs, the power spectra are estimated by computing periodograms and averaged over all K realizations of the network's dynamics. In order to monitor sudden changes in the topologies of the networks, five characteristic statistics are calculated:

- (1) The mean degree (the average number of vertices attached to the nodes) $\langle k \rangle$ of the associated undirected graphs, described by the symmetrized adjacency matrix $\mathbf{A}^s = \Theta(\mathbf{A} + \mathbf{A}^T)$, where Θ denotes Heaviside's step function.
- (2) The total distribution

$$d(l) = \frac{\text{tr}(\mathbf{A}^l)}{L\mathcal{N}}, \quad (12)$$

of cycles of length l [2,8–10,23,44,46]. In Eq. (12), $\text{tr}(\mathbf{A}^l)$ provides the total number of (not necessarily self-avoiding) closed paths of length l through the network. Since any node at such a path may serve as the starting point and there are l nodes, the correct number of cycles is obtained by dividing by l . Finally, $\mathcal{N} = \sum_l \text{tr}(\mathbf{A}^l)/l$ is a normalization constant.

- (3) From the cycle distribution, we derive an order parameter s for topological transitions by the averaged slopes of the envelope of $d(l)$, where the envelopes are estimated by connecting the local maxima of $d(l)$. Over each complete evolution cycle, the values

$$s_{\text{sub}} = \min_{s < 0} s,$$

$$s_{\text{crit}} = \min_{s > 0} s,$$

$$s_{\text{super}} = \max_{s > 0} s, \quad (13)$$

are determined.

- (4) The global excitation

$$G_{\text{ex}} = \sum_{j^+} w_{ij}^+ \quad (14)$$

and

- (5) inhibition

$$G_{\text{in}} = \sum_j w_{ij}^- \quad (15)$$

of the nodes.

The whole procedure is repeated for each network size $M = 10$ times where we have chosen $L_{200} = 400, L_{500} = 800$, and $L_{1000} = 1600$ iterations of network evolution.

4. Results

Figs. 1–3 display typical representatives of the simulations for three different phases of the networks' evolution. These phases are determined by the smallest negative (Fig. 1), the smallest positive (Fig. 2) and the largest positive (Fig. 3) value of the cycle order parameter s , averaged over the $M = 10$ network simulations, that are presented in Table 1. We refer to the first phase as the *subcritical* one $\langle s_{\text{sub}} \rangle$, to the second as the *critical phase* $\langle s_{\text{crit}} \rangle$ and to the third as the *supercritical phase* $\langle s_{\text{super}} \rangle$. The respective values are determined with Eqs. (13).

Additionally, Tables 2–4 present the averaged mean degrees, mean excitation and mean inhibition corresponding to the subcritical, critical, and supercritical phase, respectively.

The characteristic network representatives m_{crit} displayed in Figs. 1–3 are obtained by the optimization

$$m_{\text{crit}} = \arg \min_{1 \leq m \leq M} |s(m) - \langle s_{\text{crit}} \rangle|, \quad (16)$$

where $s(m)$ denotes the order parameter for the m th realization for each network size N . Fig. 1 shows representative time series (a), power spectra (b) and total cycle distributions, $d(l)$ (Eq. (12)), (c) for the subcritical phase. For all network sizes we observe a relaxation of the model EEG E (Fig. 1(a)) settling down in fixed point attractors after transients. For $N = 200, 500$ the stable

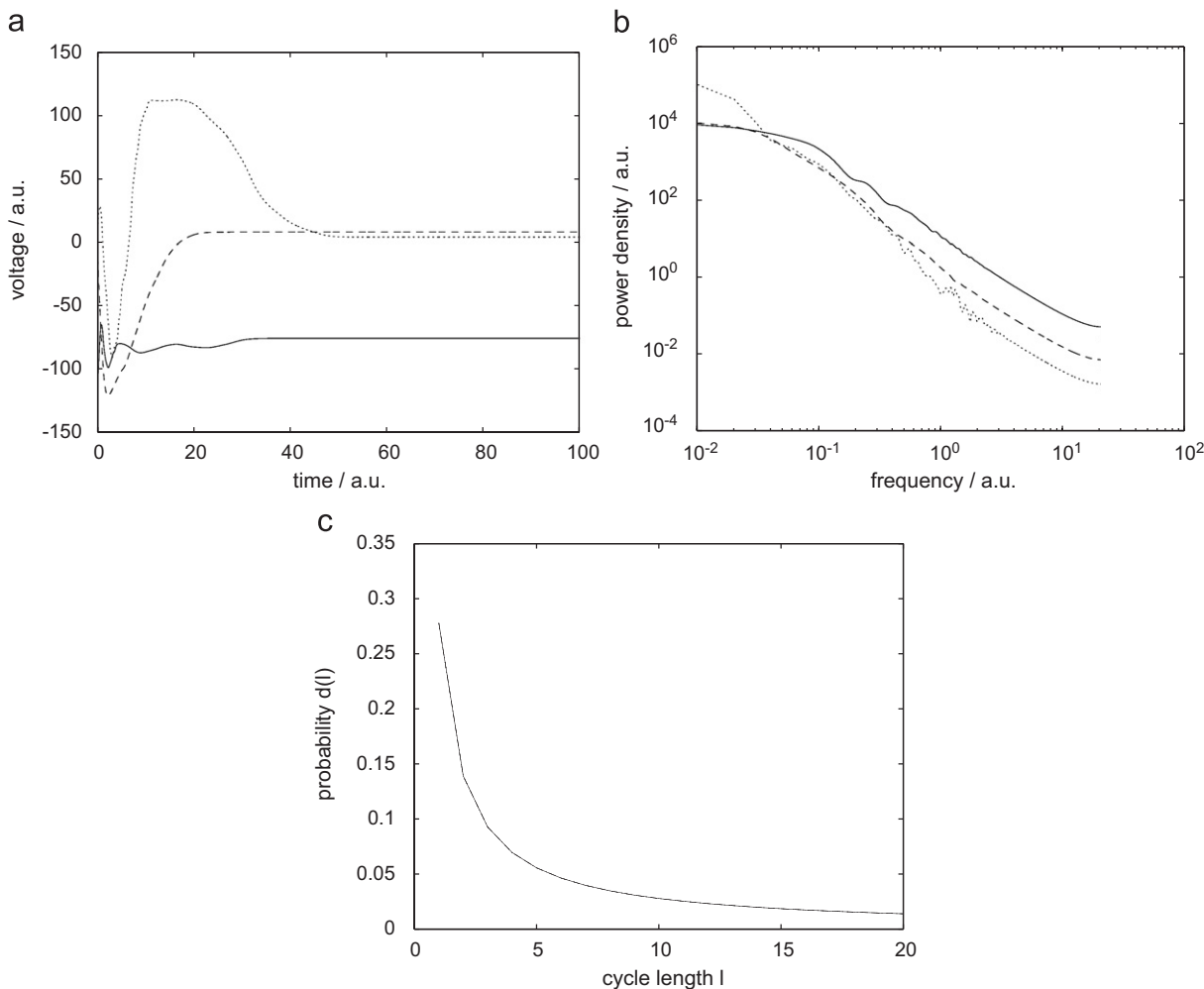


Fig. 1. (a) Representative simulated time series before the oscillatory transition (subcritical phase) for three different network sizes: $N = 200$ (dotted), $N = 500$ (dashed), and $N = 1000$ (solid). (b) Power spectra of simulated time series. (c) Total distributions of cycles (Eq. (12)) for the same networks.

state is around $E = 0$ whereas for $N = 1000$, $E \approx -70$. This can be explained by the cycle distributions Fig. 1(c). They exhibit a geometric decay, indicating the presence only of loops of length one as the numerator of Eq. (12) is constant while the denominator increases with l . A loop of length one corresponds to a non-vanishing diagonal weight $w_{ii} \neq 0$ in Eq. (6). Therefore, the stationary solutions obey

$$V_i^* = w_{ii} \tanh V_i^*, \quad (17)$$

i.e. they are the fixed points of the hyperbolic tangent.

The relaxation of the model EEG is also reflected by the power spectrum in Fig. 1(b). Since the fixed points V_i^* of Eq. (17) are exponentially approached without sufficient input from the other nodes, the “power spectrum” is simply the transfer function given by the absolute square of the Laplace transform $1/(2\pi i f + \tau^{-1})$ of the exponential $\exp(-t/\tau)$, thus accounting for the broad-band continuum with the approximated $1/f$ tail observed in the simulations (Fig. 1(a)).

Fig. 2 shows the same three network representatives m_{crit} in the critical phase when sudden oscillations occur in the node’s dynamics (as shown in Fig. 2(a) and indicated by the peaks in the power spectra (Fig. 2(b))). These oscillations can be speculatively regarded as the “alpha waves” of the model. The cycle distributions $d(l)$ (Fig. 2(c)) display a transition from geometrically decaying to exponentially growing functions that is indicated by the small values of $\langle s_{\text{crit}} \rangle$ in Table 1.

Finally, Fig. 3 displays these networks late after the oscillatory transition in the supercritical phase. The power spectra (Fig. 3(b)) display a broad $1/f$ continuum whose tail is again attributed to the relaxation properties of the leaky integrator neurons (Eq. (6)). By contrast, the $1/f$ behavior, now present at small frequencies, is due to the appearance of sustained transients as shown in Fig. 3(a) for $N = 500, 1000$, which are also characteristic for real EEG oscillations. These transients are more or less periodic which is reflected by the peaks in the power spectrum Fig. 3(b). The cycle distributions $d(l)$ (Fig. 3(c)) are all growing exponentials after the transition.

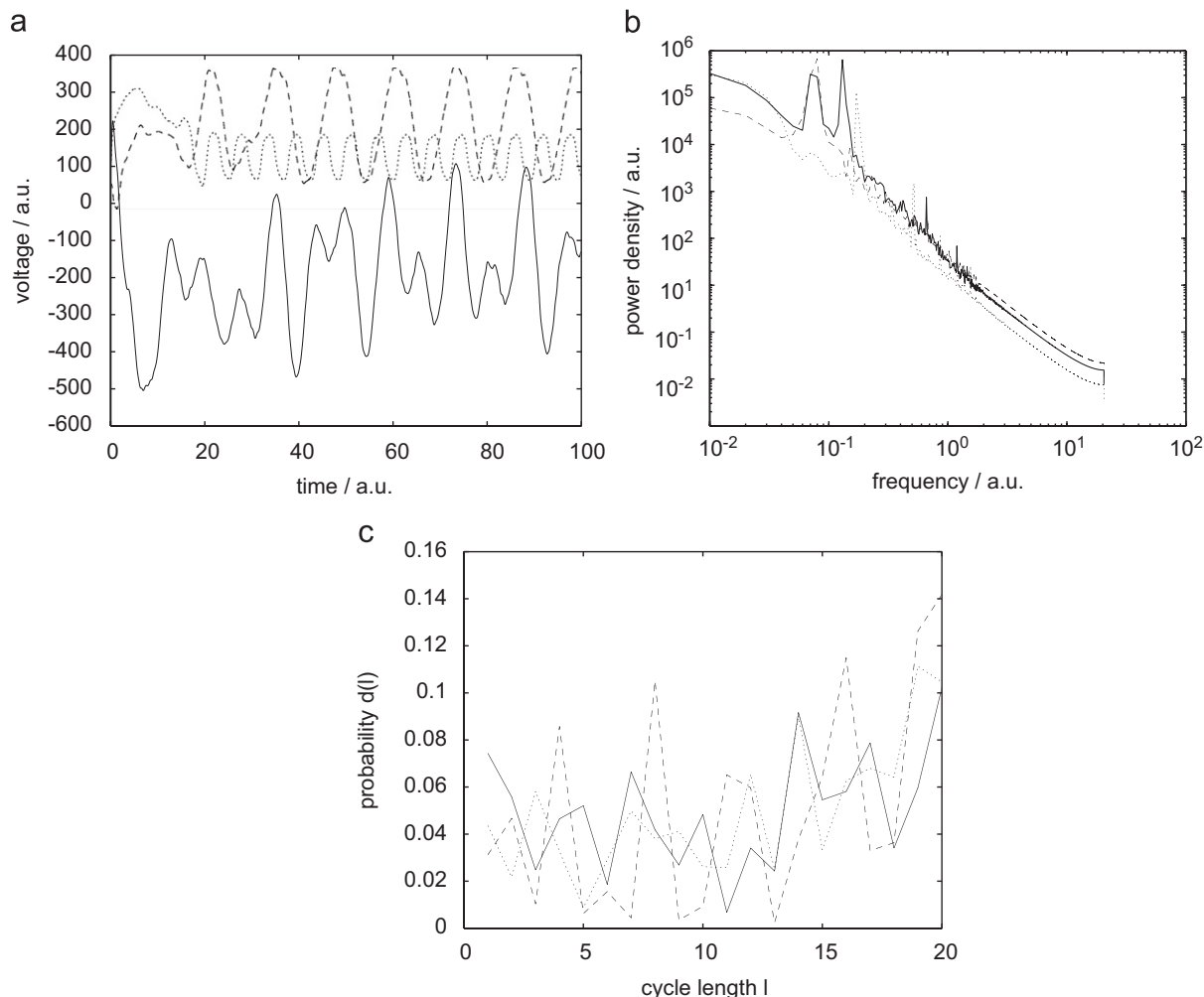


Fig. 2. (a) Representative simulated time series during the oscillatory transition (critical phase) for three different network sizes: $N = 200$ (dotted), $N = 500$ (dashed), and $N = 1000$ (solid). (b) Power spectra of simulated time series. (c) Total distributions of cycles (Eq. (12)) for the same networks.

5. Discussion

Our results are robust among all M simulations. For the network sizes $N = 200, 500, 1000$, a multitude of dynamic behavior is possible, including multistability and limit cycles. The oscillatory transition occurs for critical mean degrees of $\langle k_{\text{crit}} \rangle_{200} = 2.34$, $\langle k_{\text{crit}} \rangle_{500} = 2.28$ and $\langle k_{\text{crit}} \rangle_{1000} = 2.30$ (cf. Table 2). According to random graph theory, Erdős–Rényi graphs exhibit a percolation transition when a giant cluster suddenly occurs for $\langle k \rangle = 1$ [2,10,9]. A second transition takes place for $\langle k \rangle = 2$ indicating the appearance of mainly isolated cycles in the graph. Isolated cycles are characterized by a geometrically decaying envelope of the total cycle distribution. Our simulations suggest the existence of a third important transition when super-cycles are composed from merging smaller ones. This is reflected by a transition of the total cycle distribution $d(l)$ from a geometrically decaying to an exponentially growing behavior due to a “combinatorial explosion” of possible self-intersecting paths through the network (super-cycles are common in regular lattices with $\langle k \rangle \geq 3$). We detect this transition by means of a suitably chosen order parameter s

derived from $d(l)$ as the averaged slope of its envelope. For decaying $d(l)$, $s < 0$ and for growing $d(l)$, $s > 0$. The appearance of super-cycles is associated with $s \approx 0$ if $d(l)$ (Table 1) is approximately symmetric in the range of l . In this case, sustained oscillations emerge in the network’s dynamics.

The oscillatory transition is also reflected by a global excitation-to-inhibition ratio $G_{\text{ex}}/G_{\text{in}}$ of about -13 for $N = 200$ and -16 for $N = 500, 1000$ in the critical phase (cf. Tables 3 and 4). This is consistent with findings on the balance between excitation and inhibition [49]. The oscillatory regime persists in the supercritical phase as long as the number of excitatory connections remains balanced by the stronger weights of the inhibitory connections. If too many excitatory loops are created, the dynamics again saturates in the fixed points of Eq. (17).

The present study is a first attempt towards nonlinear complex neural network models of the brain (for related linear models, cf. [46,27]). It opens several directions for future research, including more appropriate models of electrophysiology [56,5] and brain development [46,29] where one could utilize better fitting evolution dynamics

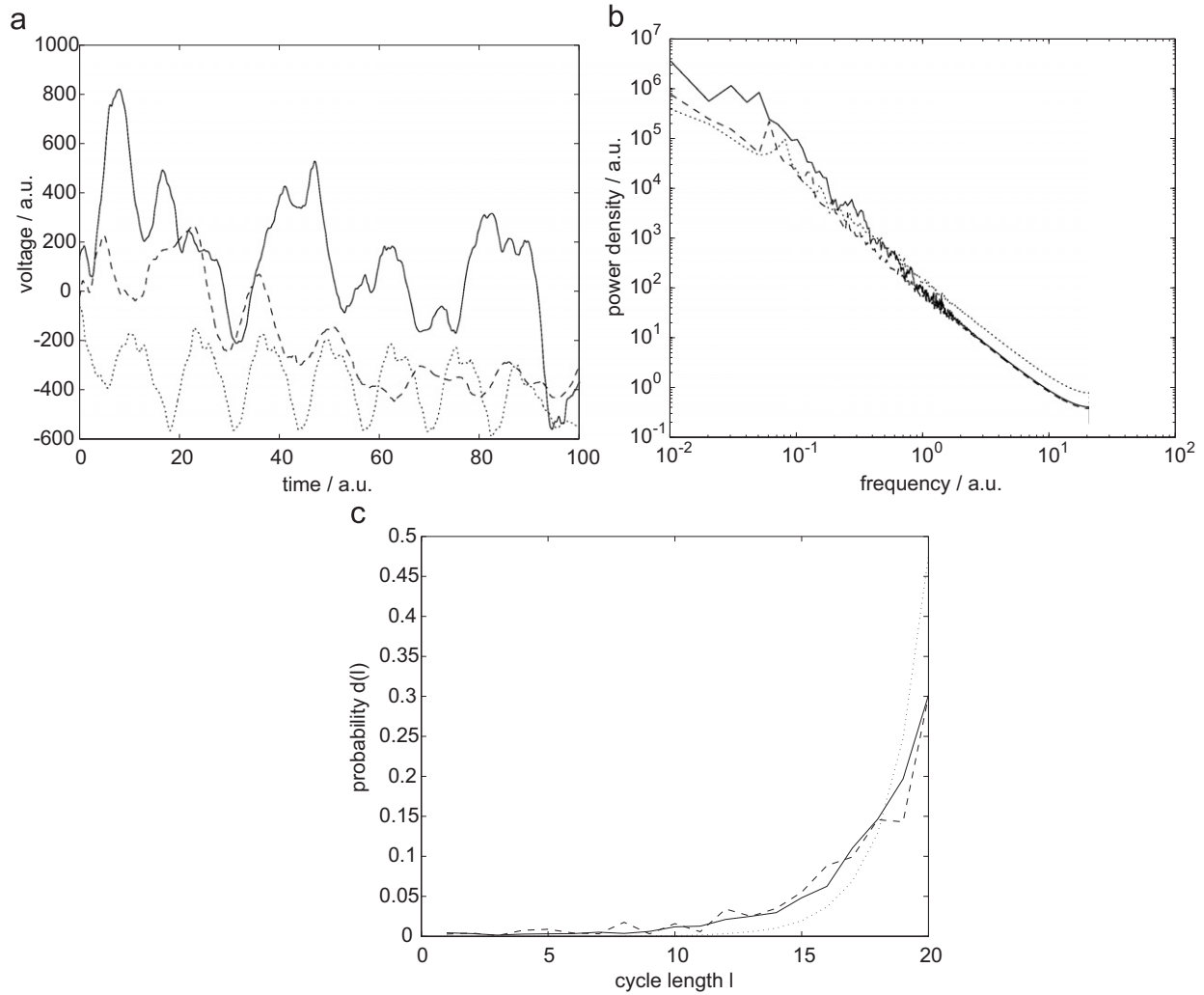


Fig. 3. (a) Representative simulated time series after the oscillatory transition (supercritical phase) for three different network sizes: $N = 200$ (dotted), $N = 500$ (dashed), and $N = 1000$ (solid). (b) Power spectra of simulated time series. (c) Total distributions of cycles (Eq. (12)) for the same networks.

Table 1
Averaged subcritical, critical, and supercritical values of the cycle order parameter s for the three network sizes

N	$\langle s_{\text{sub}} \rangle$	$\langle s_{\text{crit}} \rangle$	$\langle s_{\text{super}} \rangle$
200	-0.01396	0.00375	0.01785
500	-0.01361	0.00282	0.01345
1000	-0.01052	0.00198	0.01256

Table 3
Averaged subcritical, critical, and supercritical values of the global excitation G_{ex} for the three network sizes

N	$\langle G_{\text{ex,sub}} \rangle$	$\langle G_{\text{ex,crit}} \rangle$	$\langle G_{\text{ex,super}} \rangle$
200	355.6	730.8	1166.0
500	1092.4	1847.2	2343.2
1000	2180.8	3693.2	4605.6

Table 2
Averaged subcritical, critical, and supercritical mean degrees $\langle k \rangle$ for the three network sizes

N	$\langle k_{\text{sub}} \rangle$	$\langle k_{\text{crit}} \rangle$	$\langle k_{\text{super}} \rangle$
200	1.16	2.34	3.68
500	1.34	2.28	2.89
1000	1.36	2.30	2.87

Table 4
Averaged subcritical, critical, and supercritical values of the global inhibition G_{in} for the three network sizes

N	$\langle G_{\text{in,sub}} \rangle$	$\langle G_{\text{in,crit}} \rangle$	$\langle G_{\text{in,super}} \rangle$
200	-27.4	-53.7	-82.1
500	-61.8	-109.7	-139.6
1000	-135.7	-230.1	-284.7

that leads to small world or scale-free networks [2,10]. Also an interplay between the slow weight and the fast node dynamics could be incorporated by Hebbian correlation learning rules [15] in order to describe synaptic plasticity. Finally, one could speculate about implementing cognitive processes by emergent neural oscillations [56,33,6,37,19].

In order to further improve the physiologic plausibility of the model, time constants, gain factors and firing thresholds, i.e. the parameters τ_i , β_i , and θ_i in Eqs. (5) and (6), have to be chosen accordingly. Actually, they should be heterogeneously distributed for accounting to the inhomogeneity of biological neural networks.

Acknowledgments

We gratefully acknowledge helpful discussions with W. Ehm, P. Franaszczuk, A. Hutt, V.K. Jirsa, T. Liebscher, and J.J. Wright, as well as the support by the *Deutsche Forschungsgemeinschaft* (research group “Conflicting Rules in Cognitive Systems”) and by the Helmholtz Institute for Supercomputational Physics at the University of Potsdam.

References

- [1] S.M. Ahn, W.J. Freeman, Steady-state and limit cycle activity of mass of neurons forming simple feedback loops (I): lumped circuit model, *Kybernetik* 16 (1974) 87–91.
- [2] R. Albert, A.-L. Barabási, Statistical mechanics of complex networks, *Rev. Mod. Phys.* 74 (1) (2002) 47–97.
- [3] D.J. Amit, Modeling Brain Function. The World of Attractor Neural Networks, Cambridge University Press, Cambridge, MA, 1989.
- [4] E. Başar, M. Özgören, S. Karakaş, C. Başar-Eroğlu, Super-synergy in brain oscillations and the grandmother percept is manifested by multiple oscillations, *Int. J. Bifurcat. Chaos* 14 (2) (2004) 453–491.
- [5] C. Bédard, H. Kröger, A. Destexhe, Modeling extracellular field potentials and the frequency-filtering properties of extracellular space, *Biophys. J.* 86 (3) (2004) 1829–1842.
- [6] P. beim Graben, B. Jurish, D. Saddy, S. Frisch, Language processing by dynamical systems, *Int. J. Bifurcat. Chaos* 14 (2) (2004) 599–621.
- [7] J.M. Berrie, W.J. Freeman, M. Lenhart, Spatiotemporal analysis of prepyriform, visual, auditory, and somesthetic surface EEGs in trained rabbits, *J. Neurophysiol.* 76 (1996) 520–539.
- [8] G. Bianconi, A. Capocci, Number of loops of size h in growing scale-free networks, *Phys. Rev. Lett.* 90 (7) (2003).
- [9] B. Bollobás, Random Graphs, volume 73 of Cambridge Studies in Advanced Mathematics, second ed., Cambridge University Press, Cambridge, UK, 2001.
- [10] S. Bornholdt, H.G. Schuster (Eds.), Handbook of Graphs and Networks. From the Genome to the Internet, Wiley, Weinheim, 2003.
- [11] O. Creutzfeld, J. Houchin, Neuronal basis of EEG-waves, in: Handbook of Electroencephalography and Clinical Neurophysiology, vol. 2, part C, Elsevier, Amsterdam, 1974, pp. 2C-5–2C-55.
- [12] O. David, D. Cosmelli, K.J. Friston, Evaluation of different measures of functional connectivity using a neural mass model, *NeuroImage* 21 (2004) 659–673.
- [13] O. David, K.J. Friston, A neural mass model for MEG/EEG: coupling and neuronal dynamics, *NeuroImage* 20 (2003) 1743–1755.
- [14] O. David, L. Harrison, K.J. Friston, Modelling event-related responses in the brain, *NeuroImage* 25 (2005) 756–770.
- [15] P. Dayan, L.F. Abbott, Theoretical Neuroscience, Computational Neuroscience, MIT Press, Cambridge, MA, 2001.
- [16] W.J. Freeman, Mass Action in the Nervous System, Academic Press, New York, NY, 1975.
- [17] W.J. Freeman, Simulation of chaotic EEG patterns with a dynamic model of the olfactory system, *Biol. Cybern.* 56 (1987) 139–150.
- [18] W.J. Freeman, Tutorial on neurobiology: from single neurons to brain chaos, *Int. J. Bifurcat. Chaos* 2 (3) (1992) 451–482.
- [19] M. Garagnani, T. Wennekers, F. Pulvermüller, A neuronal model of the language cortex, *Neurocomputing* (2006), in press, doi:10.1016/j.neucom.2006.10.076.
- [20] J. Hertz, A. Krogh, R.G. Palmer, Introduction to the Theory of Neural Computation, Lecture Notes of the Santa Fe Institute Studies in the Science of Complexity, vol. I, Perseus Books, Cambridge, MA, 1991.
- [21] A.L. Hodgkin, A.F. Huxley, A quantitative description of membrane current and its application to conduction and excitation in nerve, *J. Physiol.* 117 (1952) 500–544.
- [22] R. Huerta, M. Rabinovich, Reproducible sequence generation in random neural ensembles, *Phys. Rev. Lett.* 93 (2004).
- [23] S. Itzkovitz, R. Milo, N. Kashtan, G. Ziv, U. Alon, Subgraphs in random networks, *Phys. Rev. E* 68 (2003).
- [24] B.H. Jansen, V.G. Rit, Electroencephalogram and visual evoked potential generation in a mathematical model of coupled cortical columns, *Biol. Cybern.* 73 (1995) 357–366.
- [25] B.H. Jansen, G. Zouridakis, M.E. Brandt, A neurophysiologically-based mathematical model of flash visual evoked potentials, *Biol. Cybern.* 68 (1993) 275–283.
- [26] V.K. Jirsa, Information processing in brain and behavior displayed in large-scale scalp topographies such as EEG and MEG, *Int. J. Bifurcat. Chaos* 14 (2) (2004) 679–692.
- [27] V.K. Jirsa, M. Ding, Will a large complex system with time delays be stable?, *Phys. Rev. Lett.* 93 (7) (2004).
- [28] V.K. Jirsa, H. Haken, Field theory of electromagnetic brain activity, *Phys. Rev. Lett.* 77 (5) (1996) 960–963.
- [29] M. Kaiser, C.C. Hilgetag, Spatial growth of real-world networks, *Phys. Rev. E* 69 (2004).
- [30] W. Klimesch, M. Schabus, M. Doppelmayr, W. Gruber, P. Sauseng, Evoked oscillations and early components of event-related potentials: an analysis, *Int. J. Bifurcat. Chaos* 14 (2) (2004) 705–718.
- [31] C. Koch, I. Segev (Eds.), Methods in Neuronal Modelling. From Ions to Networks, Computational Neuroscience, second ed., MIT Press, Cambridge, MA, 1998.
- [32] R. Kozma, M. Puljic, P. Balister, B. Bollobás, W.J. Freeman, Phase transitions in the neuropercolation model of neural populations with mixed local and non-local interactions, *Biol. Cybern.* 92 (2005) 367–379.
- [33] T. Liebscher, Modeling reaction times with neural networks using leaky integrator units, in: K. Jokinen, D. Heylen, A. Nijholt (Eds.), Proceedings of 18th Twente Workshop on Language Technology, TWLT, vol. 18, University of Twente, Twente, NL, 2000, pp. 81–94.
- [34] D.T.J. Liley, D.M. Alexander, J.J. Wright, M.D. Aldous, Alpha rhythm emerges from large-scale networks of realistically coupled multicompartmental model cortical neurons, *Network Comput. Neural Syst.* 10 (1999) 79–92.
- [35] F.H. Lopes da Silva, A. Hoeks, H. Smits, L.H. Zetterberg, Model of brain rhythmic activity: the alpha-rhythm of the thalamus, *Kybernetik* 15 (1974) 27–37.
- [36] F.H. Lopes da Silva, A. van Rotterdam, P. Bartels, E. van Heusden, W. Burr, Models of neuronal populations: the basic mechanisms of rhythmicity, in: M.A. Corner, D.F. Swaab (Eds.), Perspectives of Brain Research, Progress in Brain Research, vol. 45, 1976, pp. 281–308.
- [37] A. Maye, M. Werning, Temporal binding of non-uniform objects, *Neurocomputing* 58 (2004) 941–948.
- [38] W.S. McCulloch, W. Pitts, A logical calculus of ideas immanent in nervous activity, *Bull. Math. Biophys.* 5 (1943) 115–133.
- [39] R. Milo, S. Shenn-Orr, S. Itzkovitz, N. Kashtan, D. Chklovskii, U. Alon, Network motifs: simple building blocks of complex networks, *Science* 298 (2002) 824–827.

- [40] P.L. Nunez, R. Srinivasan, *Electric Fields of the Brain: The Neurophysics of EEG*, second ed., Oxford University Press, New York, 2006.
- [41] G. Pfurtscheller, EEG rhythms—event related desynchronization and synchronization, in: H. Haken, H.P. Koepchen (Eds.), *Rhythms in Physiological Systems*, Springer Series in Synergetics, vol. 55, Springer, Berlin, 1991, pp. 289–296.
- [42] C.J. Rennie, P.A. Robinson, J.J. Wright, Effects of local feedback on dispersion of electrical waves in the cerebral cortex, *Phys. Rev. E* 59 (3) (1999) 3320–3329.
- [43] P.A. Robinson, C.J. Rennie, J.J. Wright, H. Bahramali, E. Gordon, D.L. Rowe, Prediction of electroencephalic spectra from neurophysiology, *Phys. Rev. E* 63 (2001) 021903.
- [44] H.D. Rozenfeld, J.E. Kirk, E.M. Bollt, D. ben Avraham, Statistics of cycles: how loopy is your network?, *J. Phys. A: Math. Gen.* 38 (2005) 4589–4595.
- [45] E.-J. Speckmann, C.E. Elger, Introduction to the neurophysiological basis of the EEG and DC potentials, in: E. Niedermeyer, F. Lopez da Silva (Eds.), *Electroencephalography. Basic Principles, Clinical Applications, and Related Fields*, 4th ed., Lippincott Williams and Wilkins, Baltimore, 1999, pp. 15–27 (Chapter 2).
- [46] O. Sporns, G. Tononi, G.M. Edelman, Theoretical neuroanatomy: relating anatomical and functional connectivity in graphs and cortical connection matrices, *Cerebral Cortex* 10 (2) (2000) 127–141.
- [47] R. Srinivasan, Internal and external neural synchronization during conscious perception, *Int. J. Bifurcat. Chaos* 14 (2) (2004) 825–842.
- [48] M. Timme, F. Wolf, T. Geisel, Topological speed limits to network synchronization, *Phys. Rev. Lett.* 92 (7) (2004).
- [49] A.J. Trevelyan, O. Watkinson, Does inhibition balance excitation in neocortex?, *Prog. Biophys. Mol. Biol.* 87 (2005) 109–143.
- [50] A. van Rotterdam, F.H. Lopes da Silva, J. van den Ende, M.A. Viergever, A.J. Hermans, A model of the spatial-temporal characteristics of the alpha rhythm, *Bull. Math. Biol.* 44 (2) (1982) 283–305.
- [51] F. Wendling, F. Bartolomei, J.J. Bellanger, P. Chauvel, Epileptic fast activity can be explained by a model of impaired GABAergic dendritic inhibition, *Eur. J. Neurosci.* 15 (2002) 1499–1508.
- [52] F. Wendling, J.J. Bellanger, F. Bartolomei, P. Chauvel, Relevance of nonlinear lumped-parameter models in the analysis of depth-EEG epileptic signals, *Biol. Cybern.* 83 (2000) 367–378.
- [53] H.R. Wilson, J.D. Cowan, Excitatory and inhibitory interactions in localized populations of model neurons, *Biophys. J.* 12 (1972) 1–24.
- [54] J.J. Wright, D.T.J. Liley, Dynamics of the brain at global and microscopic scales: neural networks and the EEG, *Behav. Brain Sci.* 19 (1996) 285–320.
- [55] J.J. Wright, D.T.L. Liley, Simulation of electrocortical waves, *Biol. Cybern.* 72 (1995) 347–356.
- [56] J.J. Wright, C.J. Rennie, G.J. Lees, P.A. Robinson, P.D. Bourke, C.L. Chapman, E. Gordon, D.L. Rowe, Simulated electrocortical activity at microscopic, mesoscopic, and global scales, *Neuropsychopharmacology* 28 (2003) S80–S93.
- [57] J.J. Wright, C.J. Rennie, G.J. Lees, P.A. Robinson, P.D. Bourke, C.L. Chapman, E. Gordon, D.L. Rowe, Simulated electrocortical activity at microscopic, mesoscopic, and global scales, *Int. J. Bifurcat. Chaos* 14 (2) (2004) 853–872.
- [58] C. Zhou, J. Kurths, Hierarchical synchronization in complex networks with heterogeneous degrees, *Chaos* 16 (2006) 015104.



Peter beim Graben is a Senior Research Fellow in the Department of Clinical Language Sciences at the University of Reading. He studied physics and philosophy at the University of Hamburg and received his Ph.D. in physics at the University of Potsdam in 2000. From 2000 until 2006 he worked as a Research Associate at the Institute of Linguistics and at the Interdisciplinary Center for Dynamics of Complex Systems at the University of Potsdam within the DFG Research Group “Conflicting Rules in Cognitive

Systems”. His main background is in the theory of nonlinear dynamical systems, in particular symbolic dynamics applied for analyzing and modeling language processing-related brain potentials. He conducts classes on neurophysics, neuroimaging techniques and data analysis, and computational psycholinguistics.



Jürgen Kurths is a professor for Theoretical Physics/Nonlinear Dynamics at the University of Potsdam since 1994. He studied mathematics at the University of Rostock from 1971 until 1975 and received his Ph.D. in 1983. From 1975 to 1991 he had several affiliations at institutions for astrophysics. From 1991 to 1996 he was director of the working group “Nonlinear Dynamics” of the Max-Planck-Gesellschaft. Among others, Jürgen Kurths was a speaker of the DFG Research Group “Conflicting Rules in Cognitive

Systems” from 2002 until 2006, and he is a steering committee member of the Network of Excellence BIOSIM (EU) since 2005. He belongs to the editorial boards of *International Journal of Bifurcation and Chaos*, *Springer-Series Synergetics*, *International Journal of Complex Systems Research*, *CHAOS*, and *Nonlinear Processes in Geoscience* as an Executive Editor.